e-J. Surf. Sci. Nanotech. Vol. 13 (2015) 256-260 Conference - ISSS-7 -

Phase Coexistence in Two-Dimensional $Fe_{0.70}Ni_{0.30}$ Films on W(110)*

T. O. Menteş,† A. Sala, and A. Locatelli
Elettra - Sincrotrone Trieste S.C.p.A., Basovizza, Trieste 34149, Italy

E. Vescovo
National Synchrotron Light Source, Brookhaven National Laboratory, Upton, New York 11973, USA

J. M. Ablett
Synchrotron Soleil, L'orme des Merisiers, Saint-Aubin, BP 48, Gif-sur-Yvette F-91192, France

M. A. Niño
IMDEA Nanoscience, Campus Universitario de Cantoblanco, Madrid 28049, Spain
(Received 31 December 2014; Accepted 15 May 2015; Published 30 May 2015)

Using low energy electron microscopy, diffraction and x-ray photoemission electron microscopy, we study the phase separation in an Fe-Ni alloy film on W(110) at around 30 at.%Ni and at monolayer thickness. At high temperature, the monolayer-thick alloy is shown to transform into a biphase with submicron regions of different surface density exhibiting (1×1) and (1×8) structures. The former is pseudomorphic to the bcc substrate, whereas the latter is a slightly-distorted hexagonal adlayer lattice reminiscent of an fcc(111) monolayer. The stoichiometries of the two monolayer phases are $Fe_{0.85}Ni_{0.15}$ and $Fe_{0.58}Ni_{0.42}$ in laterally resolved x-ray photoemission microscopy measurements, with the bcc phase rich in Fe compared to the fcc one. This heterogeneous surface can be viewed as the two-dimensional limit of the bcc-fcc phase separation observed in thick films and in bulk Fe–Ni near the same composition. The length scale associated with the lateral heterogeneity in the monolayer film is much larger than the one observed in bulk alloys, suggesting that surface transport is the key mechanism in the kinetics of the phase separation process. [DOI: 10.1380/ejssnt.2015.256]

Keywords: Iron; Nickel; Alloy; Low-energy electron microscopy (LEEM); Surface structure, morphology, roughness, and topography

I. INTRODUCTION

Fe–Ni alloys have attracted considerable attention within the entire composition range due to their interesting structural and magnetic properties. Below 400°C, the Fe–Ni phase diagram displays the bcc structure at high Fe content, fcc phases at high Ni content, and a miscibility gap at around 30% Ni [1, 2]. This latter region in the phase diagram, at which there is a tendency towards phase decomposition, includes in particular the Invar alloy [3, 4]. The sensitive coupling between structure and magnetism, as seen in the Invar effect, makes the study of phase decomposition crucial in understanding the magnetic properties of Fe–Ni alloys.

Observation of the phase separation in $Fe_{1-x}Ni_x$ at around $x \approx 0.3$ is hampered due to the suppressed diffusion within bulk crystals. The length scale associated to the decomposition was reported to be about 50 nm after keeping the sample at 400°C for 1 year [2]. Besides the difficulties in the microscopy measurements due to the short length scales of crystal rearrangements in the bulk, such experiments demand extremely long observation times. In order to overcome this limitation, we grow the Fe–Ni alloy in the form of a supported thin film and exploit surface diffusion to enhance the phase separation process. In this work we concentrate on monolayer-thick Fe–Ni on W(110), which represents the two-dimensional limit of the thin-film alloy, and investigate in particular the chemical and structural homogeneity of $Fe_{0.70}Ni_{0.30}$ monolayer. Results on thicker films will be reported elsewhere [5].

In the present study, tungsten is chosen as the substrate, because it does not mix with either Fe or Ni at the temperatures considered, below 400°C. On the other hand, the considerable mismatch between W and Fe (about 10%), and W and Ni (about 27% along [001], 4% along $[1\bar{1}0]$) gives an important role to the epitaxial strain. Moreover, the bcc substrate symmetry may alter the fcc-bcc phase boundaries in the alloy diagram. The following is an account of the structural phase coexistence in the Fe–Ni monolayer at high temperature, and the identification of the modifications in the phase diagram at this two-dimensional limit in the presence of substrate interactions. The compositions are measured using laterally-resolved x-ray absorption spectroscopy measurements. The results in the current work demonstrate that the phase decomposition behaviour in the single layer film at high temperature is similar to that observed in thicker films and in bulk Fe–Ni alloy. Thus, $Fe_{0.70}Ni_{0.30}$ monolayer on W(110) provides a model for studies on the metastability of Fe–Ni alloys in two dimensions.

II. EXPERIMENTAL

The growth and characterization of the alloy films were performed at the Nanospectroscopy beamline (Elettra Sincrotrone Trieste) using the Spectroscopic PhotoEmission and Low-Energy Electron Microscope (SPELEEM) [6, 7]. The capability to perform laterally-resolved electron backscattering (Low-Energy Electron

* This paper was presented at the 7th International Symposium on Surface Science, Shimane Prefectural Convention Center (Kunibiki Messe), Matsue, Japan, November 2-6, 2014.
† Corresponding author: tevfik.mentes@elettra.eu

Microscopy, LEEM) [8, 9] and x-ray photoemission (X-ray PhotoEmission Electron Microscopy, XPEEM) [10] measurements provides a complete structural and chemical map of a given surface area with high spatial resolution of about 10 nm in LEEM and 30 nm in XPEEM. In addition, by imaging the back-focal plane, Low-Energy Electron Diffraction (LEED) data can be collected from micron-sized regions.

The W(110) substrate was cleaned by annealing to 1100°C in 1×10^{-6} mbar of oxygen followed by high temperature flashes in UHV to desorb the oxygen. The Fe–Ni alloy films were obtained by codeposition of Fe and Ni from separate e-beam evaporators. The desired alloy composition was obtained by precalibrating the evaporators via the respective monolayer completion of each element on the W(110) crystal. The pressure in the microscope chamber was lower than 3×10^{-10} mbar during growth and measurements. The sample annealing was done by electron bombardment using a tungsten filament mounted at a distance of about one millimeter on the backside of the sample. The temperature was measured using a W–Re thermocouple attached to the Mo support disk underneath the tungsten crystal.

The monolayer (ML) coverage unit is taken to correspond to a pseudomorphic monolayer matching the atomic density of the W(110) substrate. In the following, ML units will be used with this in mind, unless otherwise specified.

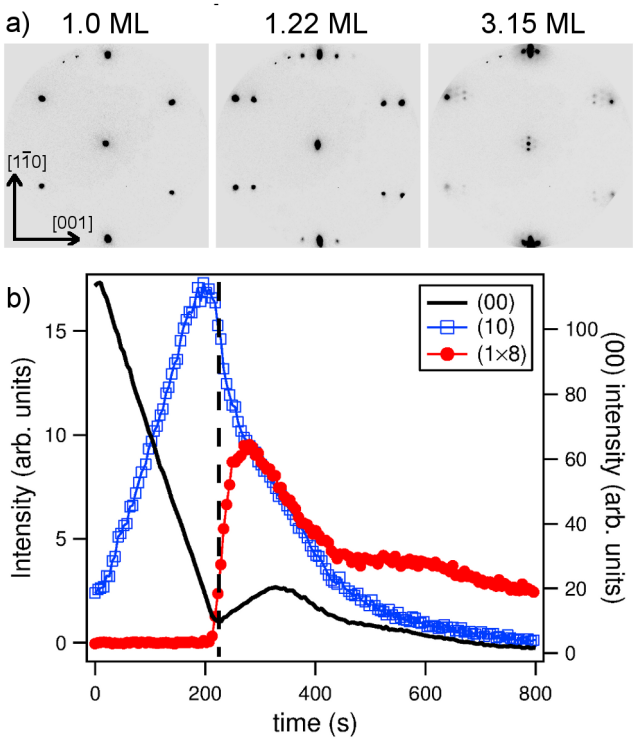

FIG. 1. $Fe_{0.70}Ni_{0.30}$ growth on W(110) at room temperature. a) LEED patterns as a function of coverage. The coverages are given in ML units pseudomorphic to W(110). b) The evolution of the LEED spot intensities during deposition. The vertical dashed line marks a total coverage of 1 ML according to the calibrations of the Fe and Ni evaporators. Electron energy is 42 eV for all the LEED data displayed.

III. RESULTS AND DISCUSSION

The growth of $Fe_{0.70}Ni_{0.30}$ films on W(110) was carried out at room temperature. The evolution of the surface structure during growth was monitored using LEED. Figure 1a) shows the LEED patterns observed in the low coverage range. Until the completion of nearly one pseudomorphic monolayer, indicated by the vertical dashed line in Fig. 1b), only the substrate pattern can be seen. Nevertheless, there is a pronounced change in spot intensities in a linear fashion, indicating the growth of a flat monolayer. At a total alloy coverage slightly below one pseudomorphic monolayer an additional pattern appears, which is identified by the (1×8) structure. The (1×8) intensity sharply rises with increasing coverage up to 1.12 ML, almost saturates above this coverage, and forms a broad peak at about 1.22 ML. At this coverage, the (00) beam appears elongated along the [1$\bar{1}$0] direction. Upon further growth, the elongation continuously increases as new superstructure spots appear along [1$\bar{1}$0] as seen in the rightmost pattern in Fig. 1a). At higher coverages than those displayed in the figure, this additional structure transforms into one that matches the well-known periodic dislocation network observed in Fe films of similar coverage on W(110) [11].

The observation of the (1×8) pattern just above 1.0 ML coverage is very similar to the behaviour of a pure Ni layer on W(110) at the same coverages [12, 13]. From kinematic LEED, we find that the spot positions of the alloy superstructure agree to within 1.5% with that of (1×8)-Ni/W(110). On the other hand, in the case of Ni/W(110), upon further deposition the layer transforms to a (1×7) structure with higher packing density along the [001] direction [14], which is not seen in the growth of the Fe–Ni alloy film.

The layer with 30% at. Ni at a total coverage of 1.18 ML is shown in Fig. 2. After growth at room temperature, a sharp (1×8) pattern is visible in LEED (Fig. 2a)). Real space imaging at high resolution shows a weak contrast modulation with slightly elongated features. The same modulation is also observed in dark-field LEEM, seen in Fig. 2b), by imaging with a (1×8) spot. In dark-field LEEM an aperture is inserted in the diffraction plane to select a particular diffraction spot. The real-space image obtained in this way maps out the structural domains giving rise to that particular spot. This somewhat striped surface with a nearly-periodic texture has an average feature size of 37 nm. No corresponding chemical heterogeneity is observed in XPEEM imaging, although the limited lateral resolution in XPEEM prohibits a conclusive statement. Therefore, the presence of a chemical modulation following the small structural domains is possible. However, a complete separation into Fe and Ni regions can be ruled out, as the (1×8) regions cover more than half the surface, which is more than what 30% Ni can provide.

The thermal stability of the alloy monolayer was monitored in LEEM during annealing. No changes are observed during a gradual temperature increase up to about 300°C. Above this temperature, the surface becomes heterogeneous below the 1 μm scale as shown in Fig. 2c)-f). The surface morphology is maintained upon cooling

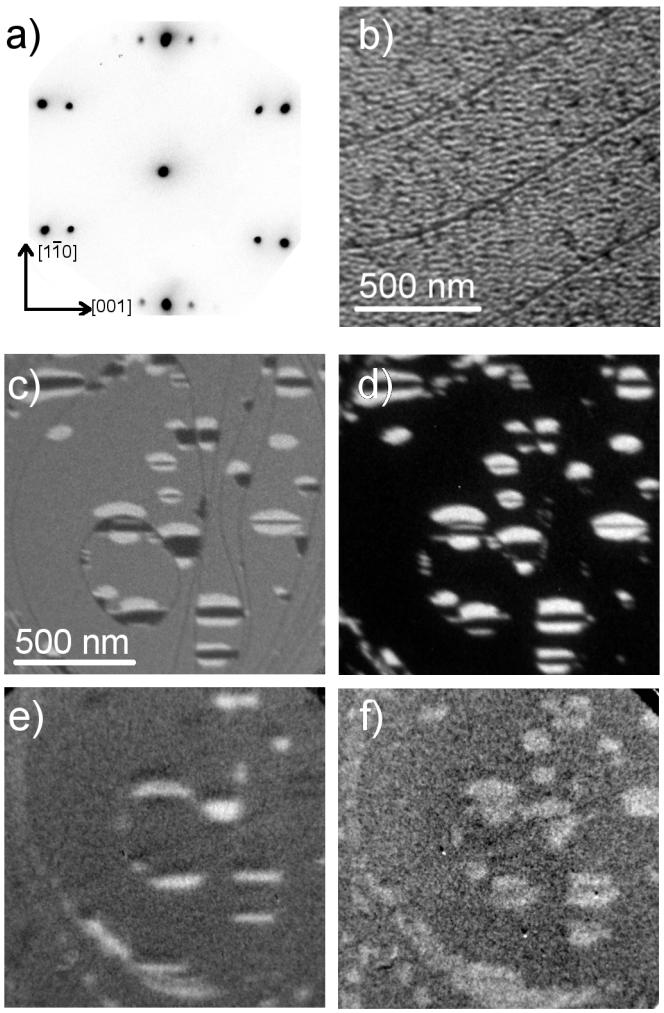

FIG. 2. The structure of the 1.18 ML $Fe_{0.7}Ni_{0.3}$ film on W(110) before and after annealing. a) LEED, b) dark-field LEEM show the presence and the distribution of the (1×8) structure on the surface after room temperature growth. The surface upon annealing to 330 C° as seen by c) LEEM (17 eV electron energy), d) dark field LEEM (1×8 spot, 45 eV), e) XAS-PEEM at the Fe L_3 edge, f) XAS-PEEM at the Ni L_3 edge. The images are acquired after cooling down to room temperature. The surface morphology remains the same during cool-down as monitored by LEEM.

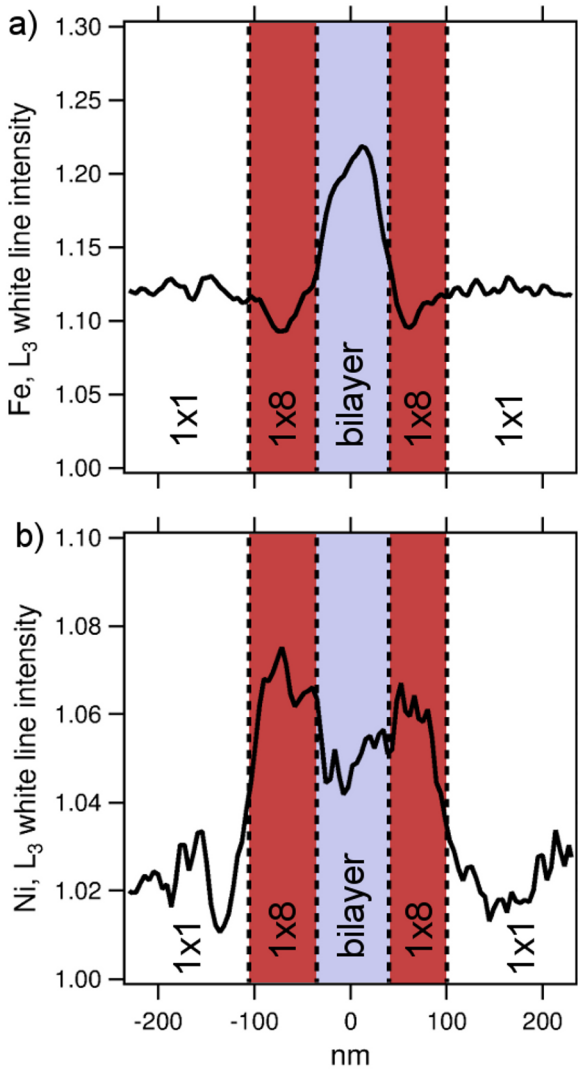

FIG. 3. XAS white line intensity of (a) Fe L_3, (b) Ni L_3, across a profile, which goes through all three structural regions. The different regions are marked on the plot. The y axis reflects the secondary emission intensity at the L_3 peak normalized to the baseline intensity acquired at a photon energy 5 eV lower than the absorption threshold.

down the sample. The fast cooling rate and the suppressed diffusivity at lower temperatures evidently allow to freeze the high-temperature morphology down to the measurement temperature. The heterogeneity consists of three distinct structural regions as clearly observed in Fig. 2c), with bright and dark elongated features within the homogeneous gray background. Dark-field LEEM in Fig. 2d) reveals that only one type of island has the (1×8) structure. The majority of the surface shows the pseudomorphic pattern. This is a direct indication that the (1×1) bcc monolayer is energetically favored in comparison to denser layer structures. Using dark-field LEEM (not shown), the dark regions in Fig. 2c) are identified with extra LEED spots near the (00) beam as seen also in the rightmost panel in Fig. 1a).

In order to assess the lateral composition of the various phases, we performed x-ray absorption spectromicroscopy measurements at room temperature. The lateral distributions of Fe and Ni are displayed in Fig. 2e) and f). The images are obtained by dividing the secondary electron image at the photon energy equal to the corresponding L_3 absorption threshold by the image acquired at a photon energy below the absorption threshold. In other words, the images are lateral maps of the white line intensity of the Fe or Ni L_3 resonance normalized to the baseline intensity. In Fig. 3, these quantities are plotted along a spatial profile across a typical island and its surroundings featuring all three structural domains. The signal levels, consistent with the LEED superstructure, indicate that the dark islands in Fig. 2c) are multilayer regions as opposed to the single layer film everywhere else. The formation of the multilayer islands upon annealing is not surprising considering that Fe and Ni ultrathin films on W(110) were reported to break into islands at about

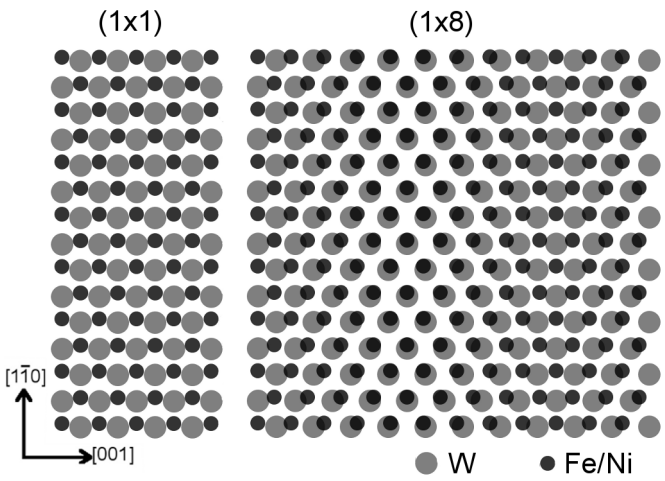

FIG. 4. Schematic top view of the pseudomorphic and (1×8) monolayer structures of Fe–Ni on W(110). The (1×1) sketch allows for a small in-plane displacement along $[1\bar{1}0]$ following the calculation of pseudomorphic Ni on W(110) [14]. The (1×8) structure, instead, simply represents the 12.5% contraction along [001], neglecting the expected lateral displacements of adatoms within the unit cell.

500 K and 600 K, respectively [15].

From the intensity ratios of the Fe and Ni signals in the two regions, along with the respective densities (i.e. (1×8) has 12.5% more material than the pseudomorphic monolayer), the compositions of the (1×1) and (1×8) areas are found to be $Fe_{0.85}Ni_{0.15}$ and $Fe_{0.58}Ni_{0.42}$, respectively. The errors in the composition determination are relatively large (≥ 0.03) due to the low signal-to-noise ratio.

In order to discuss the results on the Fe–Ni alloy adlayer reported above, in Fig. 4 we give the sketches of the pseudomorphic and (1×8) layers on W(110). In the (1×1) structure, the adatoms are slightly displaced along $[1\bar{1}0]$ from the bridge site, in order to schematically account for the adsorption site in the pseudomorphic Ni layer on W(110) [14].

Regarding the (1×8) Ni/W(110), there has not yet been any detailed structural study reported in the literature. It is known that this superstructure is due to an atomic density 12.5% higher along the [001] direction for the adlayer compared to the substrate [13], which is the basis of the sketch in Fig. 4. We should note that a recent study on the (1×7) Ni/W(110) (similar to, but denser than, the (1×8) layer) revealed that the lattice is not simply contracted homogeneously along [001], but there are significant displacements of the adatoms within the large surface unit cell [14]. We expect a similar situation for both the Ni/W(110) and Fe–Ni/W(110) (1×8) structures. Nevertheless, on average the 12.5% contraction along [001] brings the adlayer to a nearly-hexagonal network as it can be appreciated in Fig. 4.

Therefore, we can view the (1×8) islands in Fig. 2c)-f) as the two-dimensional limit of a strained fcc lattice. This coexistence of bcc-like and fcc-like Fe–Ni monolayer structures at 330 °C brings to mind the boundaries of the metastability region in the Fe–Ni bulk phase diagram at the same temperature, which correspond to about $Fe_{0.7}Ni_{0.3}$ (bcc) and $Fe_{0.5}Ni_{0.5}$ (fcc) [2]. As shown previously, the compositions for the Fe–Ni monolayer regions on W(110) are $Fe_{0.85}Ni_{0.15}$ $(1 \times 1$, bcc) and $Fe_{0.58}Ni_{0.42}$ $(1 \times 8$, fcc-like), which are close to the values from the bulk phase diagram.

Based on these measured alloy stoichiometries, there is a slight shift in the metastability phase boundaries towards Fe-rich compositions going to the two-dimensional limit (x is 0.3/0.5 in bulk vs 0.15/0.42 in monolayer). Such a shift can be, at least in part, attributed to the relatively large experimental errors. On the other hand, the presence of the substrate is expected to modify the phase diagram at the ultra-thin limit. Indeed, the thermal desorption studies in the literature give a bonding energy for the Ni monolayer on W(110) of 3.4 eV/atom [17], which is lower than the corresponding value for Fe of 4.1 eV/atom [16]. In other words, the tungsten substrate favors the presence of Fe in the monolayer phase. This suggests, though in speculative terms, that in the two-dimensional case the metastability region of the Fe–Ni phase diagram shifts towards higher Fe content due to the interactions with the W substrate.

As seen in Fig. 2, the length scale at which the monolayer alloy separates within minutes is above 100 nm at 330 °C. As we have suggested earlier, these length and time scales are respectively longer and shorter than those observed for bulk samples [2]. The suppressed mobility in the bulk crystal can be understood as the result of a *cage effect* [18]. In other words, the freedom of motion in three-dimensions is highly limited due to the crystalline order. Therefore, diffusion in bulk proceeds via the vacancies and interstitials within the lattice. Importantly, the self-interstitial formation energy in the bcc Fe lattice is more than 3 eV [19]. On the other hand, the diffusion barriers, both for bulk vacancies and interstitials [19] and for surface adatoms [20], are generally about or below 1 eV. In the past, experiments took advantage of high-energy ion irradiation in order to create bulk defects and thus to facilitate phase separation [21]. Instead, in the current work, we show that the phase separation can be induced at relatively large distances and short times going to the two-dimensional limit, at which surface diffusion enhances the decomposition process.

At this point, the question arises on the nature of the stripe pattern observed after room temperature growth as seen in Fig. 2b). There is a distinct difference between this modulated surface at the nanoscale, and the phase-separated surface upon high temperature annealing. The high temperature phase results by nucleation and growth of (1×8) islands at a much longer length scale. Instead, during room temperature deposition, the nearly-periodic stripe pattern forms everywhere all at once. We attribute this low-temperature pattern to the spinodal decomposition of the unstable $Fe_{0.7}Ni_{0.3}$ layer into metastable phases, in which the structural modulation is possibly accompanied by a chemical inhomogeneity, though below our detection limit. The high temperature structural coexistence marks the boundaries of the metastable phase, with the compositions mentioned above. A discussion of the metastability and the spinodal region can be found in Ref. [22].

IV. SUMMARY

In conclusion, an Fe–Ni alloy monolayer with nominal concentration around 30 at.%Ni has been prepared on a W(110) substrate at room temperature by simultaneous evaporation from elemental Fe and Ni. Annealed at temperatures above 300°C, the monolayer separates into submicron regions corresponding to two distinct phases, structurally and compositionally di-homogeneous: a (1×1) pseudomorphic bcc $Fe_{0.85}Ni_{0.15}$ phase and a (1×8) quasi-hexagonal fcc $Fe_{0.58}Ni_{0.42}$ one. In spite of the strong lattice mismatch between the W(110) substrate and these Fe–Ni alloys, the phase separation in monolayer-thick films appears to be similar to that observed in thick films and in bulk Fe–Ni near the same composition. The formation of this heterogeneous surface can therefore be considered as the two-dimensional limit of the bcc-fcc phase separation expected in a bulk system. Moreover, the length scale at which the separation takes place is considerably larger than the one seen in bulk alloys, indicating that the surface transport controls the kinetics of the separation process.

[1] K. B. Reuter, D. B. Williams, and J. I. Goldstein, Metall. Trans. A **20**, 711 (1989).
[2] J. Zhang, D. B. Williams, and J. I. Goldstein, Metall. Mat. Trans. A **25**, 1627 (1994).
[3] R. J. Weiss, Proc. Phys. Soc. **82**, 314 (1963).
[4] M. van Schilfgaarde, I. A. Abrikosov, and B. Johansson, Nature **400**, 46 (1999).
[5] T. O. Menteş *et al.*, in preparation.
[6] A. Locatelli, L. Aballe, T. O. Menteş, M. Kiskinova, and E. Bauer, Surf. Interface Anal. **58**, 1554 (2006).
[7] T. O. Menteş, G. Zamborlini, A. Sala, and A. Locatelli, Beilstein J. Nanotechnol. **5**, 1873 (2014).
[8] E. Bauer, Rep. Prog. Phys. **57**, 895 (1994).
[9] M. S. Altman, J. Phys.: Condens. Matter **22**, 084017 (2010).
[10] A. Locatelli and E. Bauer, J. Phys.: Condens. Matter **20**, 093002 (2008).
[11] U. Gradmann and G. Waller, Surf. Sci. **116**, 539 (1982).
[12] J. Kołaczkiewicz and E. Bauer, Surf. Sci. **144**, 495 (1984).
[13] D. Sander, C. Schmidthals, A. Enders, and J. Kirschner, Phys. Rev. B **57**, 1406 (1998).
[14] N. Stojić and N. Binggeli, J. Phys.: Condens. Matter **24**, 135001 (2012).
[15] P. J. Berlowitz and D. W. Goodman, J. Vac. Sci. Technol. A **6**, 634 (1988).
[16] P. J. Berlowitz, J.-W. He, and D. W. Goodman, Surf. Sci. **231**, 315 (1990).
[17] Z. Yang and R. Wu, Surf. Sci. **469**, 36 (2000).
[18] W. Kob and H. C. Andersen, Phys. Rev. E **48**, 4364 (1993).
[19] C.-C. Fu, F. Willaime, and P. Ordejón, Phys. Rev. Lett. **92**, 174403 (2004).
[20] D. Reuter, G. Gerth, and J. Kirschner, Phys. Rev. B **57**, 2520 (1998).
[21] F. A. Garner, J. M. McCarthy, K. C. Russell, and J. J. Hoyt, J. Nucl. Materials **205**, 411 (1993).
[22] K. Binder, Phys. Rep. **50**, 783 (1987).